





Magnetic separation of metal sulfides/oxides by Fe_3O_4 at room temperature and atmospheric pressure

Jia-Hui Ji, Yi-Fei Xiao, Bin Shen, Qiu-Ying Yi, Jin-Long Zhang* ,
Ming-Yang Xing* 

Received: 25 December 2018/Revised: 14 January 2019/Accepted: 27 February 2019/Published online: 3 April 2019
© The Nonferrous Metals Society of China and Springer-Verlag GmbH Germany, part of Springer Nature 2019

Abstract The recovery of heterogeneous catalysts can save costs and avoid secondary pollution, but its separation efficiency and recovery cost are limited by conventional separation methods such as precipitation–flocculation, centrifugation and filtration. In this paper, we found that surface-defective metal sulfides/oxides (WS_2 , CuS , ZnS , MoS_2 , CdS , TiO_2 , MoO_2 and ZnO) commonly used in advanced oxidation processes (AOPs) could be magnetically recovered at room temperature and atmospheric pressure by mechanically mixing with Fe_3O_4 . Zeta potential, Raman, X-ray photoelectron spectroscopy (XPS) and electro-spin resonance (ESR) spectra were measured to explore the mechanism of the magnetic separation phenomenon. The exposed active metal sites on the surface of defective metal sulfides/oxides are beneficial for the formation of chemical bonds, which are combined with electrostatic force to be responsible for the magnetic separation. Moreover, other factors affecting the magnetic separation were also investigated, such as the addition of amount of Fe_3O_4 , different solvents and particle sizes. Finally, WS_2 was chosen to be applied as a co-catalyst in Fenton reaction, which could be well separated by the magnetic Fe_3O_4 to achieve the recycle of catalyst in Fenton reaction. Our research provides a general strategy for the

recycle of metal sulfides/oxides in the catalytic applications.

Keywords Magnetic separation; Metal sulfides/oxides; Recycle; Fenton reaction

1 Introduction

During the past few decades, catalysts have played an increasingly irreplaceable role in industrial production. They can reduce the activation energy, accelerate the reaction rate or increase the selectivity of chemical reactions [1–3]. However, the practical application of homogeneous catalysts in liquid-phase reaction is restricted by high costs, difficulties in separation and recovery and formation of metal-complexing [4]. To overcome these shortcomings of homogeneous catalysts, different methods have been proposed, such as nanofiltration and new separation techniques based on liquid–liquid separation, including ionic liquids, fluorine phases, supercritical solvents and polymeric supports; however, some problems have arisen, which lead to the limitations of costs, efficiency and secondary pollution [5]. Therefore, heterogeneous catalysis is occupying a more important position gradually for the effective and environmentally friendly reactions. Different types of heterogeneous catalysts have been applied in many fields, such as the production of fine chemicals and pharmaceuticals, chemical technology and advanced oxidation processes (AOPs) [6–11]. Heterogeneous catalysts with relatively recyclable nature will save the cost, reduce the waste and make the reaction environmentally friendly, which is consistent with the strategy of sustainable development.

J.-H. Ji, Y.-F. Xiao, B. Shen, Q.-Y. Yi, J.-L. Zhang*,
M.-Y. Xing*
Key Laboratory for Advanced Materials and Institute of Fine
Chemicals, School of Chemistry and Molecular Engineering,
East China University of Science and Technology, Shanghai
200237, China
e-mail: jlzhang@ecust.edu.cn

M.-Y. Xing
e-mail: mingyangxing@ecust.edu.cn

As a robust, efficient and rapid tool to separate heterogeneous catalysts, magnetic separation has many advantages compared to those approaches like precipitation–flocculation, filtration or centrifugation. Actually, magnetic separation technology has been widely used in the mining and food processing industries for decades, via using eddy currents, electromagnets and permanent magnets to separate magnetic materials from non-magnetic materials on a wet or dry basis [12]. As an inherent part of many material handling operations, magnetic technology has undergone tremendous development over the past decades [13]. Generally, the selection of separation processes is determined by the chemical and physical properties of materials, as well as the time and energy expended. Although traditional separation methods such as centrifugal separation or filtration have been widely used, it may be the best choice for the materials with intrinsic magnetism to be separated by an applied magnetic field, which is of easy operation and convenient [14–18].

Magnetite (Fe_3O_4) is a ferrimagnetic mineral with a spinel structure containing ferric and ferrous ions occupying octahedral and tetrahedral coordination sites, respectively, whose oxygen atoms are arranged into cubes to enclose the lattice. The ferrimagnetic property of magnetite is determined by the spin arrangement in ferrous ions antiparallel to that in ferric ions, and the interactions of iron ions in different coordination sites lead to incomplete cancelation of spin moments and a strong magnetization [19]. Definitely, there are plenty types of magnetic materials, such as maghemite ($\gamma\text{-Fe}_2\text{O}_3$) and other ferrites (MFe_2O_4 , $\text{M} = \text{Co}, \text{Mn}$, etc.) [20], but the magnetism of them is much lower than that of magnetite. In addition, other magnetic metals, pure zero-valent iron (ZVI) nanoparticles, are always easy to be oxidized [21, 22]. Thereby, magnetite is the best choice to participate in magnetic separation as a support, co-catalyst or catalyst in catalytic applications.

The magnetic separation technology is applied in many fields, with the main purpose of separating non-magnetic and magnetic materials. In detail, non-magnetic materials do not interact with target magnetic materials and thus remain in the solution after magnetic materials get separated by an applied magnetic field [23, 24]. At present, only those heterogeneous catalysts who have magnetism can be recycled by an external magnetic field, so many magnetic heterogeneous catalysts have been prepared for magnetic recycled purpose. Hajian et al. [25] prepared $\text{Fe}_3\text{O}_4@\text{MCM-41-Im}@\text{MnPor}$ catalyst with tetraphenylporphyrinatomanganese(III) chloride immobilized onto imidazole functionalized MCM-41 and magnetic nanoparticle core. The prepared catalyst can be easily recovered through the application of an external magnet. The separation of the as-prepared heterogeneous catalyst was

achieved by simple magnetic decantation without obvious mass loss, so that it could be reused for the next catalysis application. Ma et al. [26] fabricated series of magnetic $\text{Fe}_3\text{O}_4/\text{TiO}_2$ composites through simple sol-gel strategy. $\text{Fe}_3\text{O}_4/\text{TiO}_2$ composites exhibited excellent magnetic recycle property because the surface of magnetic Fe_3O_4 was coated with spherical TiO_2 nanoparticles. However, the preparation of magnetic materials is complex, and there will be other pollution produced during the preparation, increasing the cost and time.

Here, we found that some commercial metal sulfides/oxides exposed with surface defects and commonly used in AOPs could be magnetic separated with Fe_3O_4 with an applied magnetic field. We systematically summarized the recoverable degrees of these metal sulfides/oxides with Fe_3O_4 added in the solution, and the mechanism of magnetic separation was explored through zeta potential, Raman, X-ray photoelectron spectroscopy (XPS) analysis and electro-spin resonance (ESR) spectra. The interactions between metal sulfides/oxides and Fe_3O_4 , such as the electrostatic force or chemical bonds, were considered to be the dominating causes when they were mixed mechanically and separated with an external magnetic field. This method is considered to be more convenient, simple and lower cost than centrifugation, filtration and preparation of magnetic materials. Therefore, magnetic separation has great potential application in the field of heterogeneous catalysts recovery, even some of which are non-magnetic. For instance, this method was successfully applied to WS_2 -Fenton reaction to recycle WS_2 after the reaction.

2 Experimental

2.1 Chemicals and reagents

All the chemicals, including tungsten (IV) sulfide (Alfa Aesar (China) Chemical Co., Ltd., 99.8%), cupric sulfide (Shanghai Macklin Biochemical Co., Ltd., analytical reagent (AR), 99.0%), zinc sulfide (Shanghai Aladdin Bio-Chem Technology Co., Ltd., 99.99%, 3.3–4.3 μm), molybdenum (IV) sulfide (Alfa Aesar (China) Chemical Co., Ltd., 99%; Shanghai Aladdin Bio-Chem Technology Co., Ltd., 99.5%, < 2 μm), cadmium sulfide (Shanghai Macklin Biochemical Co., Ltd., AR, 98%), titanium (IV) oxide (Shanghai Aladdin Bio-Chem Technology Co., Ltd., 99.8%, anatase), molybdenum (IV) oxide (Shanghai Energy Chemical Co., Ltd., 99%), zinc oxide (Shanghai Lingfeng Chemical Reagent Co., Ltd., $\geq 99\%$), triiron tetraoxide (Beijing HWRK Chem Co., Ltd., 1 μm , 99.9%), sodium hydroxide (Shanghai Titan Scientific Co. Ltd., AR, $\geq 96.0\%$), sulfuric acid (Shanghai Titan Scientific Co. Ltd., CP, 95.0%–98.0%), ferrous sulfate heptahydrate

(Shanghai Aladdin Bio-Chem Technology Co., Ltd., 99.95%), hydrogen peroxide (Shanghai Experiment Reagent Co., Ltd., 30%), cyclohexane (Shanghai Titan Scientific Co. Ltd., AR, $\geq 99.5\%$), 2-propanol (Shanghai Titan Scientific Co. Ltd., AR, $\geq 99.7\%$), ethanol (Shanghai Titan Scientific Co. Ltd., AR, $\geq 99.7\%$), were used without further purification. Deionized water (DI-water) was produced by OKP-S040 Standard ultrapure water system and applied in all the following experiments.

2.2 Experimental procedures

The magnetic separation experiments were performed in glass vials, the quality of which were weighed and recorded in advance. The fixed amount of the metal sulfide/oxide and Fe_3O_4 were mixed into 10 ml solvent while only the metal sulfide/oxide was added as a control experiment. The solution pH was adjusted and recorded. Subsequently, a magnet was placed on the side of glass vials for the magnetic separation test, and the magnetic separation time was taken down. A few seconds later, with the magnet attracting, the solvent and the part that could not be magnetic separated were emptied, and the residues were washed by the solvent once and then dried for 48 h in a vacuum drying chamber. Finally, the total masses of glass vials were weighed so that the mass of the metal sulfide/oxide separated by the magnetic field could be calculated.

The degradation experiments were performed in plastic cups with a magnetic stirring to keep the solution homogeneous during the reaction. The predesigned initial pH of RhB solution was adjusted to 4.0 first with sodium hydroxide and sulfuric acid, which was considered to be the best pH in Fenton reaction. Then, the fixed amount of WS_2 and $\text{FeSO}_4 \cdot 7\text{H}_2\text{O}$ were added into 100 ml reaction solution with desired concentration of RhB. Finally, quantitative H_2O_2 was added to initiate the oxidation. Samples were taken out at regular intervals, centrifuged and analyzed immediately. After the reaction, Fe_3O_4 was added into the solution. Then, Fe_3O_4 and WS_2 were magnetic separated by an external magnetic field.

2.3 Analytic methods

The pH values of the solution were detected with a pH meter (INESA PHS-3C). Raman spectra of metal sulfides/oxides were measured by using a Renishaw inVia spectrometer using Ar^+ laser of 532 nm at room temperature. The XPS of metal sulfides/oxides was conducted at a condition of Al K α irradiation by THERMO ESCALAB 250 Xi. Zeta potentials of metal sulfides/oxides and size distributions of MoS_2 from different manufacturers were investigated by a Zetasizer (Malvern, ZEN3600). ESR spectrometer (Bruker, 100G-18 KG/EMX-8/2.7) was used

to detect the types of defects in metal sulfides/oxides at room temperature. The concentration of RhB was measured with a ultraviolet–visible (UV–Vis) spectrophotometer (SHIMADZU UV-2450).

3 Results and discussion

3.1 Magnetic separation of different metal sulfides/oxides with Fe_3O_4 in aqueous solution

All the metal sulfides/oxides (WS_2 , CuS, ZnS, MoS_2 , CdS, TiO_2 , MoO_2 and ZnO) used in the experiments are non-magnetic. As shown in Fig. 1, no magnetic separation of any metal sulfide/oxide was observed without Fe_3O_4 added in aqueous solution. However, when Fe_3O_4 was added, the metal sulfides/oxides were separated to different degrees quickly. For instance, with Fe_3O_4 present, WS_2 , CdS and CuS were magnetically separated thoroughly, making the aqueous solution clarified; MoS_2 (Alfa), MoO_2 and ZnO seemed partial separation with some residues left; ZnS, TiO_2 and MoS_2 (Aladdin) had poor magnetic separation, resulting in turbid solutions that show no significant change compared to the solutions before magnetic separation.

Furthermore, detailed magnetic recovery rates of different metal sulfates/oxides are shown in Fig. 2a, which were consistent with the experimental phenomena in Fig. 1. Among all metal sulfides/oxides, WS_2 reached the highest magnetic recovery rate (99.0%), while CuS and CdS also performed relatively good magnetic recovery rates of 87.5% and 90.5%, respectively. The recycling rates of other metal sulfides/oxides became decreasing. Specifically, the recovery rates of MoS_2 (Alfa), MoO_2 and ZnO were 85.2%, 79.6% and 80.1%, respectively, while ZnS, TiO_2 and MoS_2 (Aladdin) only obtained the magnetic recovery rates of 69.5%, 46.8% and 43.0%, respectively. There is no doubt that Fe_3O_4 is magnetic and can be attracted with a magnetic field [27, 28], but the reason why non-magnetic metal sulfides/oxides together with Fe_3O_4 could also be separated by a magnetic field needs to be further investigated. Some kinds of interactions should be present between metal sulfides/oxides and Fe_3O_4 after mechanical mixing so that metal sulfides/oxides would follow Fe_3O_4 to be separated together while an applied magnetic field was attracting. Moreover, metal sulfides/oxides weakly interacting with Fe_3O_4 would have a relatively poor magnetic separation degree while strong interactions between them would result in a through separation from the solution.

3.2 Role of electrostatic force in magnetic separation

In view of the above-mentioned phenomena in Fig. 2, the electrostatic force between metal sulfides/oxides and Fe_3O_4

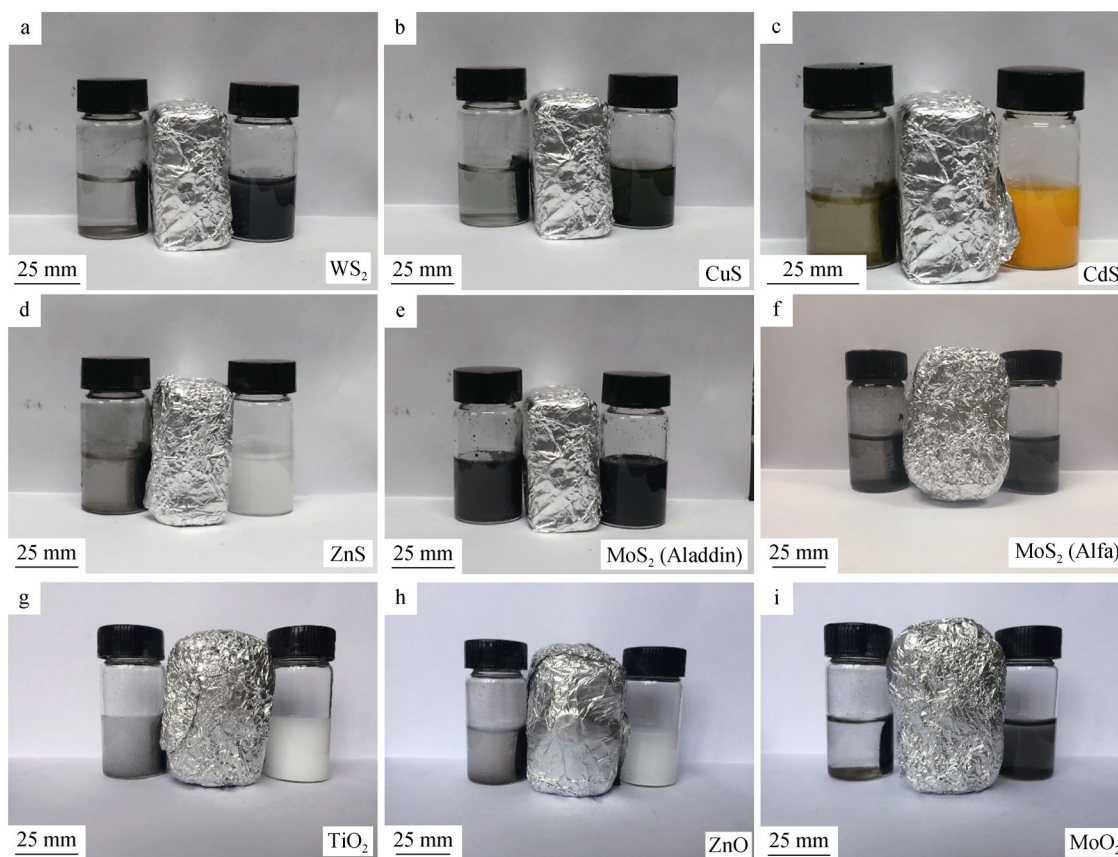


Fig. 1 Magnetic separations of different metal sulfides/oxides with Fe_3O_4 (left of each picture) and without Fe_3O_4 (right of each picture): **a** WS_2 , **b** CuS , **c** CdS , **d** ZnS , **e** MoS_2 (Aladdin), **f** MoS_2 (Alfa), **g** TiO_2 , **h** ZnO and **i** MoO_2

is the first reason worth considering, because they were just mechanically blended [29]. Therefore, zeta potential tests were taken to determine the charged states of different particle surfaces. Considering that WS_2 had the best magnetic separation rate and TiO_2 had comparatively low magnetic separation rate, they were chosen to participate in zeta potential tests. The main purpose was to explore the isoelectric points of them. As shown in Fig. 2b, the zeta potential of Fe_3O_4 was -34.7 mV at $\text{pH} = 10.84$, 6.59 mV at $\text{pH} = 5.00$ and 4.46 mV at $\text{pH} = 1.86$, respectively; the zeta potential of WS_2 was -30.3 mV at $\text{pH} = 3.23$ and -16.3 mV at $\text{pH} = 1.25$, respectively; the zeta potential of TiO_2 was -22.7 mV at $\text{pH} = 11.77$, 0.42 mV at $\text{pH} = 9.92$ and 17.4 mV at $\text{pH} = 6.10$, respectively. Therefore, the isoelectric points of Fe_3O_4 , WS_2 and TiO_2 could be speculated as follows: at pH between 5.00 and 10.84 for Fe_3O_4 , lower than 1.25 for WS_2 and near neutral for TiO_2 [30].

As shown in Fig. 2c, the pH of $\text{WS}_2/\text{Fe}_3\text{O}_4$ mixture was 3.24, at which the surfaces of WS_2 and Fe_3O_4 were charged negatively and positively, respectively, and they were magnetically separated in 3 s (Fig. 2f). When the solution pH was adjusted to 11.30, both of their surfaces became

negative. The magnetic separation time became a bit longer, but they could still be magnetically separated in 5 s (Fig. 2g), implying that there should be another kind of interaction between WS_2 and Fe_3O_4 for the magnetic separation. As shown in Fig. 2d, as for $\text{TiO}_2/\text{Fe}_3\text{O}_4$ mixture, the initial pH was 4.20, at which the surfaces of TiO_2 and Fe_3O_4 both were charged positively that may account for their poor magnetic separation rate (46.8%) (Fig. 2h). Although there was no significant variation of the magnetic separation degrees after the pH adjusted to 8.00, at which the surface of TiO_2 became positive but the surface of Fe_3O_4 remained negative, the recovery of TiO_2 had slight improvement, reaching 49.5% in Fig. 2i.

Based on above experimental results, we could draw the conclusion that the electrostatic force was one of the factors affecting the magnetic separation, not only the magnetic separation time, but also the recovery rate; however, it was not the dominant force to influence non-magnetic substances magnetically separated with Fe_3O_4 by an applied magnetic field.

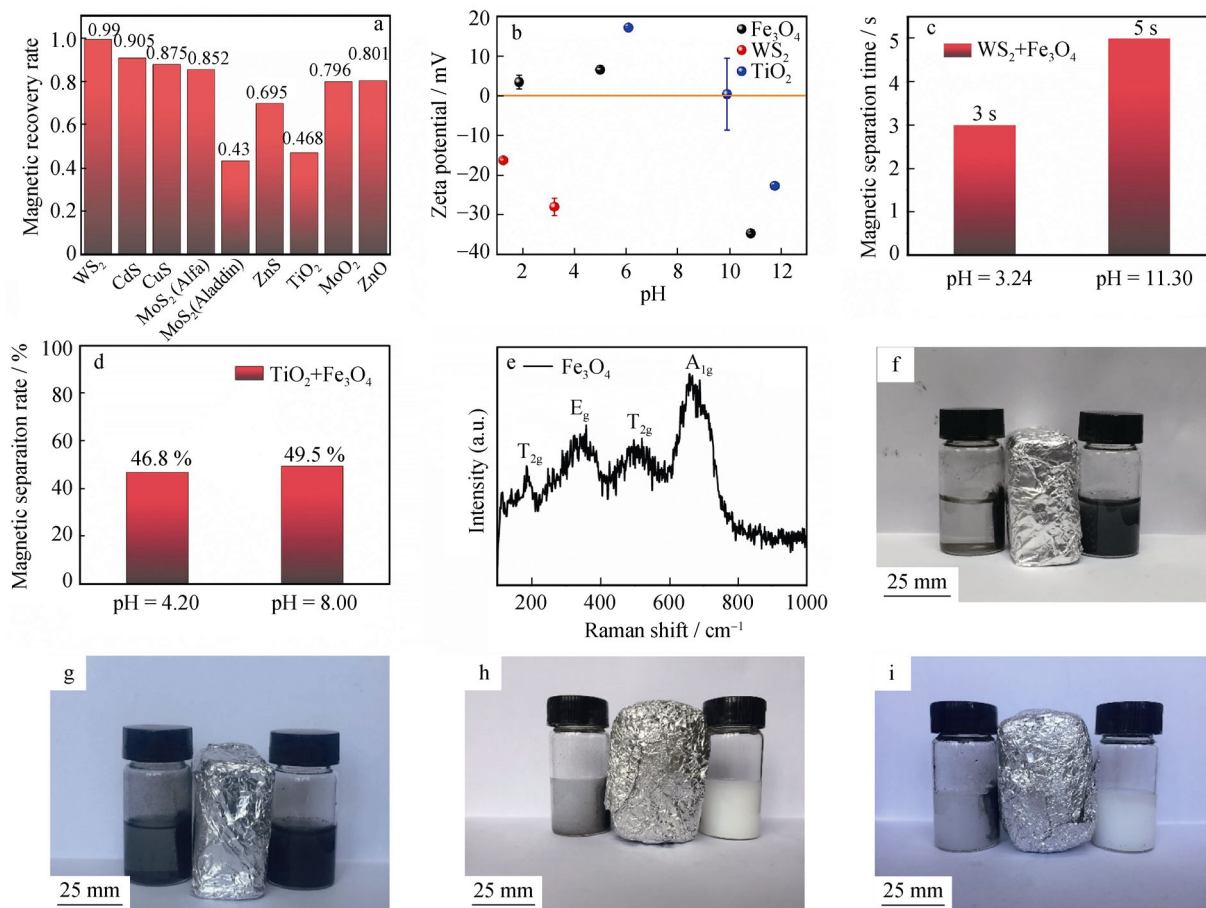


Fig. 2 **a** Magnetic recovery rate of different metal sulfides/oxides with Fe_3O_4 ; **b** zeta potential of Fe_3O_4 , WS_2 and TiO_2 at different pH; **c** variation of magnetic separation time of WS_2 and Fe_3O_4 at different pH; **d** variation of magnetic separation rate at different pH; **e** Raman spectrum of Fe_3O_4 ; variation of magnetic separation time of WS_2 and Fe_3O_4 at pH **f** 3.24 and **g** 11.30; variation of magnetic separation time of WS_2 and Fe_3O_4 at pH **h** 4.20 and **i** 8.00

3.3 Formation of chemical bonds in magnetic separation

In order to explore whether chemical bonds were established or not between metal sulfides/oxides and Fe_3O_4 after mechanical mixing, Raman, XPS and ESR spectra were employed in this case. With the same reasons as mentioned above, WS_2 and TiO_2 were chosen for primary detailed characterizations and discussions. Figures 2e and 3 show Raman spectra of magnetite and different metal sulfides/oxides before and after mixing and magnetic separation with Fe_3O_4 . As shown in Fig. 2e, the strongest magnetite band (A_{1g} mode) of Fe_3O_4 Raman spectrum was observed at 665 cm^{-1} . The other three magnetite phonon frequencies generated much smaller bands at 189 (T_{2g}), 346 (E_g) and $497\text{ (}T_{2g}\text{)}\text{ cm}^{-1}$, respectively, which were consistent with the previous report [31]. Figure 3a exhibits the Raman spectra of WS_2 with the characteristic peak at 475 cm^{-1} [32], and it was worth noting that the weak contribution appearing at 669 cm^{-1} of the mixture was referred to the

A_{1g} mode of Fe_3O_4 that was not observed on the Raman spectrum of the pure WS_2 . Moreover, the A_{1g} mode of Fe_3O_4 was blueshifted by 4 cm^{-1} compared to that of the pure Fe_3O_4 , proving that the electron clouds on the surface of Fe_3O_4 transferred to WS_2 , building the connection between Fe_3O_4 and WS_2 . The Raman spectra of pure anatase and anatase/ Fe_3O_4 mixture are shown in Fig. 3b. The black line represents the five characteristic peaks corresponding to the Raman modes of TiO_2 : E_g (144 cm^{-1}), E_g (198 cm^{-1}), B_{1g} (396 cm^{-1}), B_{1g}/A_{1g} (518 cm^{-1}) and E_g (638 cm^{-1}), respectively [33] (A_{1g} and B_{1g} are the brookite Raman peaks). Both the frequencies of B_{1g} mode and A_{1g} mode were close to 518 cm^{-1} . After the mechanical mixing and magnetic separation with Fe_3O_4 , all the peaks of TiO_2 became wider because the Raman peak positions of TiO_2 and Fe_3O_4 were close. Moreover, the E_g mode and A_{1g} mode of Fe_3O_4 were observed. The results evidenced that TiO_2 could also be magnetically separated, but the inferior separation was still confused. As for other metal sulfides/oxides (Fig. 3c–i), the A_{1g} modes of Fe_3O_4

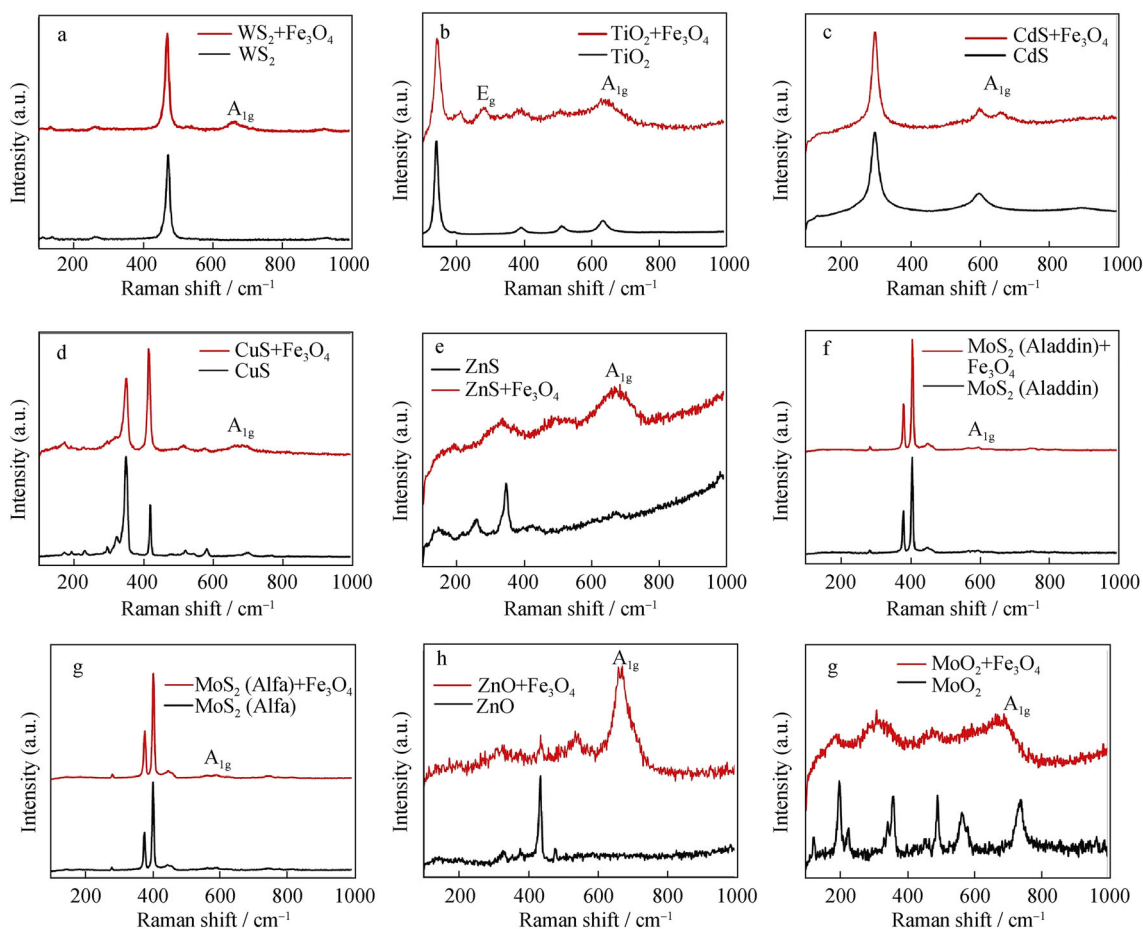


Fig. 3 Raman spectra of **a** WS₂, **b** TiO₂, **c** CdS, **d** CuS, **e** ZnS, **f** MoS₂ (Aladdin), **g** MoS₂ (Alfa), **h** ZnO, **i** MoO₂ before and after mixing and separated with Fe₃O₄

were also observed in their Raman spectra, which varied in strength and position. For instance, the A_{1g} modes in CuS and CdS Raman spectra both occurred at 663 cm⁻¹ (Fig. 3c, d), with 2 cm⁻¹ lower than that of pure Fe₃O₄, implying that the electron clouds transferred from CuS and CdS to Fe₃O₄.

XPS measurements were performed to further study the composition and surface chemical environment of metal sulfides/oxides. Figure 4a, d, g shows the survey XPS spectra of WS₂, CuS and TiO₂, respectively, before and after the mechanical mixing and magnetic separation with Fe₃O₄. W 4f and S 2p core levels of WS₂ are exhibited in Fig. 4b, c, respectively. The W 4f core level spectrum contained a doublet located at 33.3 and 35.5 eV, corresponding to W (IV) 4f_{7/2} and W (IV) 4f_{5/2}, respectively. The peaks at 36.3 and 38.9 eV were specified as W (VI) 4f_{7/2} and W (VI) 4f_{5/2}, respectively. The core level spectrum of S 2p had two peaks at 163.0 and 164.2 eV, assigned to the doublet of S 2p_{3/2} and S 2p_{1/2} states, respectively. The oxidation of surface sulfur atoms may account for the peak appeared at 169.8 eV [34–36]. After

the mechanical mixing and magnetic separation with Fe₃O₄, all the peaks of W 4f and S 2p were shifted to lower binding energy, declining by 0.3–0.5 eV, respectively, proving that the density of the electron clouds around tungsten atoms and sulfur atoms increased so that their ability to bind with electrons decreased. Furthermore, the peak area ratio of W(IV)/W(VI) increased, further verifying the results obtained from Raman spectra of WS₂: the formation of W(IV)-O-Fe between Fe₃O₄ and WS₂ was established, leading to the transformation of electrons from Fe₃O₄ to WS₂. Figure 4e shows the high-resolution XPS spectra of Cu 2p peak of CuS. The peaks at 932.0 and 951.9 eV were assigned to Cu 2p_{3/2} and Cu 2p_{1/2} of Cu–S bond, while the peaks located at 934.6 and 954.3 eV were attributed to Cu 2p_{3/2} and Cu 2p_{1/2} of Cu–O bond, suggesting the surface oxidation of CuS. The other two peaks at 943.4 and 963.0 eV were the satellite peaks. Figure 4f shows the high-resolution XPS spectra of S 2p for CuS, which could be fitted to three types of S. The two peaks at 162.1 and 163.1 eV were assigned to S–S bond of S 2p_{3/2} and S 2p_{1/2}, respectively, and the sulfide of Cu–S may

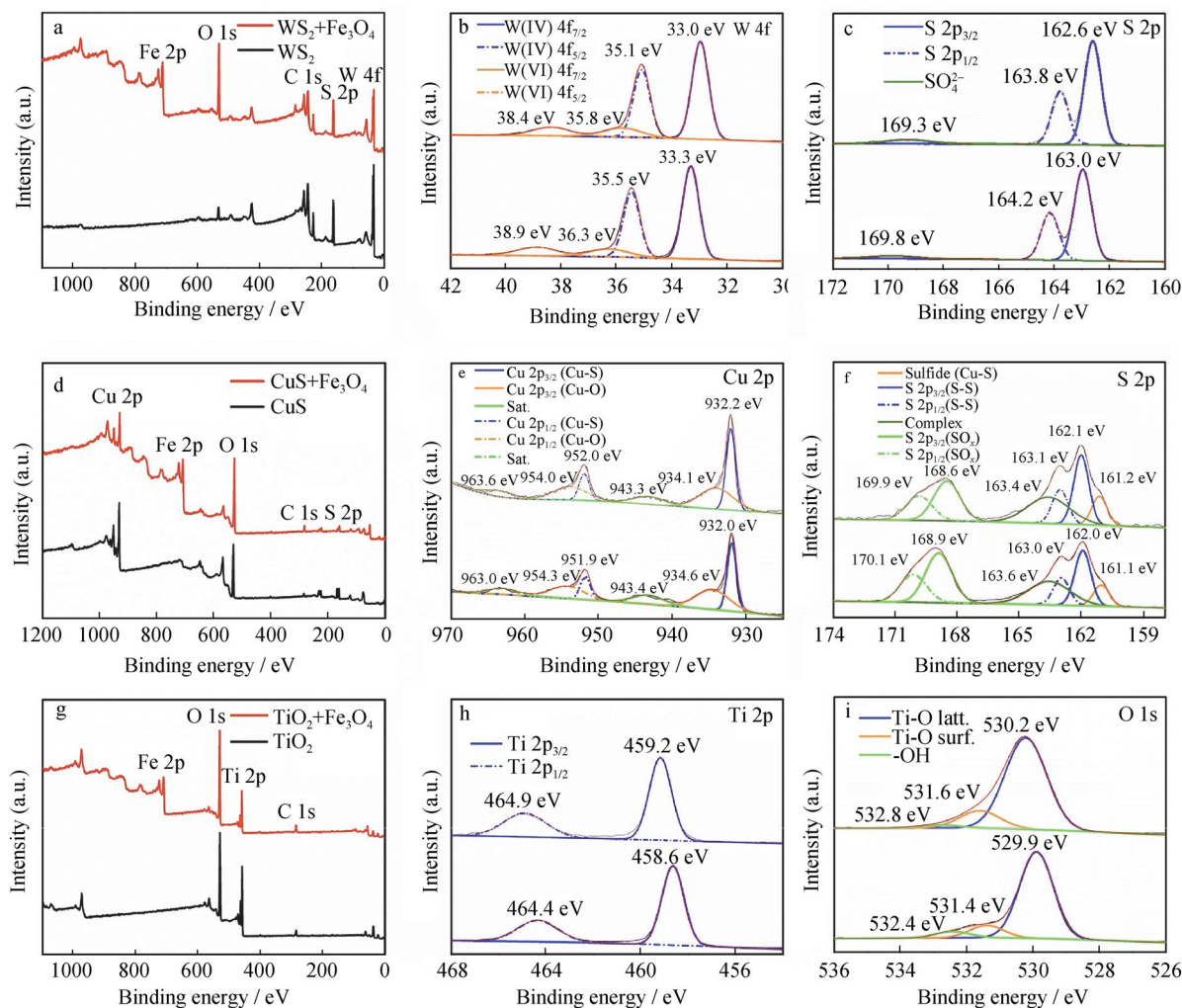


Fig. 4 XPS spectra of WS_2 : **a** survey spectrum, high-resolution spectra of **b** W 4f and **c** S 2p; XPS spectra of CuS : **d** survey spectrum, high-resolution spectra of **e** Cu 2p and **f** S 2p; XPS spectra of TiO_2 : **g** survey spectrum, high-resolution spectra of **h** Ti 2p and **i** O 1s

account for the peak at 161.0 eV, and the peaks at 168.9 and 170.1 eV were all attributed to the oxidized sulfur species of SO_x [37–39]. After the mechanical mingling and magnetic separation with Fe_3O_4 , all the peaks of Cu 2p and S 2p had slight but diverse changes. The Cu–S and S–S bonds, including Cu $2p_{3/2}$, Cu $2p_{1/2}$, S $2p_{3/2}$ and S $2p_{1/2}$, shifted to high binding energy, increasing by 0.1–0.2 eV; however, the oxidation peaks of CuS XPS spectrum became lower, declining by 0.2–0.5 eV. This phenomenon proved that the Cu(II)–O–Fe bond was formed and electrons transferred from Cu–S bonds to Fe_3O_4 , corresponding to the Raman result. Figure 4h, i shows the high-resolution XPS spectra of Ti 2p and O 1s. The two peaks of Ti 2p at 458.6 and 464.4 eV were ascribed to Ti $2p_{3/2}$ and Ti $2p_{1/2}$, respectively. Besides, the O 1s peaks could be fitted into three peaks and the binding energy at 529.9, 531.4 and 532.4 eV were referred as the lattice oxygen (Ti–O), the chemisorbed surface oxygen (Ti–O) and hydroxyl (–OH),

respectively [40]. After the mechanical mixing and magnetic separation with Fe_3O_4 , all the peaks of Ti 2p and O 1s were shifted to higher binding energy, increasing by 0.1–0.2 eV. Considering that the magnetic separation of TiO_2 with Fe_3O_4 was poor, partial TiO_2 still gets magnetically separated successfully, which was not surprising. The electrons transferred from TiO_2 to Fe_3O_4 , opposite to that of WS_2 , which may be difficult to bond toughly to Fe_3O_4 .

It is possible that the simple mechanical mixing will generate chemical bonds, for which defects on the surface of the metal sulfides/oxides may account. Theoretically, as for metal sulfides, the presence of sulfur vacancy makes it easy for oxygen atoms to fill in so that the connection between metal sulfides/oxides and Fe_3O_4 is established. Figure 5 shows the ESR spectra of WS_2 , CuS , TiO_2 , MoS_2 (Alfa) and MoS_2 (Aladdin), which were measured at room temperature. The results showed that WS_2 , MoS_2 (Aladdin)

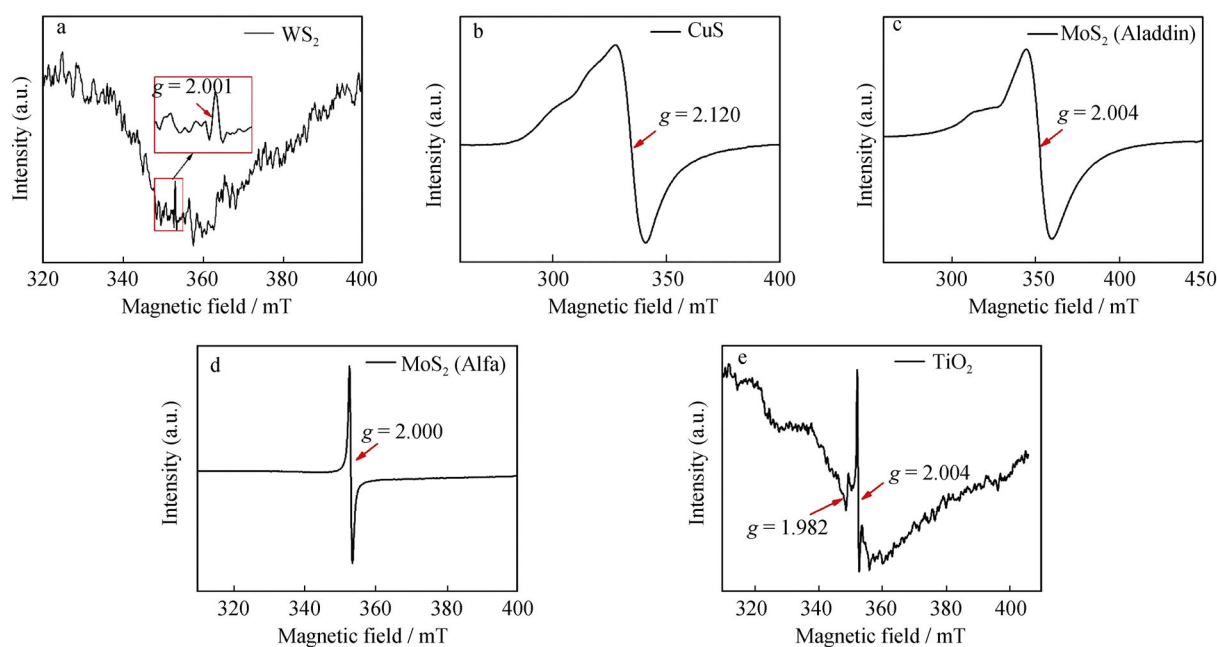


Fig. 5 Room temperature ESR spectra of **a** WS₂, **b** CuS, **c** MoS₂ (Aladdin), **d** MoS₂ (Alfa) and **e** TiO₂

and MoS₂ (Alfa) possessed a resonance signal at around $g = 2.000$ (where g is used to indicate the internal magnetic field generated by the orbital motion of unpaired electrons in the molecule.), specifically, 2.001 (Fig. 5a), 2.004 (Fig. 5c) and 2.000 (Fig. 5d), respectively. Based on recent researches, this signal was the symbol of sulfur vacancy [41, 42]. CuS had a similar signal appearing at 2.120 (Fig. 5b), considered that the sulfur vacancy was also existed in CuS [43]. As for TiO₂, Fig. 5e shows two main signals at $g = 1.982$ and $g = 2.004$ [44, 45]. The weak paramagnetic signal observed at $g = 1.982$ was the characteristic peak of Ti³⁺, while the strongest paramagnetic signal at $g = 2.004$ indicated the presence of oxygen vacancies. The existence of these defects allowed the production of chemical bonds between metal sulfides and Fe₃O₄ by simply mechanically mixing them in deionized water, due to the exposure of active metal sites on the surface of metal sulfides/oxides [46]. As mentioned above, the peak area ratio of W(IV)/W(VI) increased and the W(IV)–O–Fe bond was built. This could be explained that the oxygen atoms of Fe₃O₄ filled in the sulfur vacancy as electron donors [46] gave electrons to W(VI) and reduced partial W(VI) to W(IV). As for CuS, the oxygen atoms of Fe₃O₄ filled in the sulfur vacancy of CuS; on the one hand, the oxygen atoms were extremely electronegative, so they would attract electrons around it, increasing the binding energy of Cu–S bonds; on the other hand, as electron donors, the increase in the number of Cu–O bonds reduced their binding energy, which verified the generation of Cu(II)–O–Fe bonds. Similarly, the filling of oxygen atoms from Fe₃O₄ in the oxygen vacancy of TiO₂ attracted the

surrounding electron clouds, thus increasing the binding energy of Ti–O bonds. There must be plenty of Ti³⁺ around the oxygen vacancy and the electrons transferred from Ti³⁺ to the oxygen atoms of Fe₃O₄, resulting in the increase in the binding energy. However, the oxygen vacancy on the surface of commercial TiO₂ may be much less than the sulfur vacancy on the surface of metal sulfides, leading to the poor magnetic recovery rate.

3.4 Influence of other factors in magnetic separation

Owing to the typical magnetic separation characteristics, WS₂ and MoS₂ were selected to be typical materials to further explore the influence of other factors in magnetic separation. First, the mass ratio of Fe₃O₄ to WS₂ was investigated. Not surprisingly, the magnetic separation time decreased with the addition of Fe₃O₄ increasing. As shown in Figs. 6a–e and 7a, when the mass ratio varied from 0.5 to 2.0, the magnetic separation time decreased from 11 to 4 s. Nevertheless, only Fe₃O₄ was magnetic, so the increase in addition of Fe₃O₄ would inevitably increase the formation number of W(IV)–O–Fe bonds and therefore decrease the magnetic separation time. Moreover, WS₂ could still be separated thoroughly even with low amount of Fe₃O₄ due to the observation of clarified solutions (Fig. 6a–e). Secondly, the magnetic separation effect of mingling metal sulfides/oxides and Fe₃O₄ in organic solvents was also investigated. As shown in Fig. 6f–i, WS₂ could not be magnetically separated alone in any solvent, including deionized water, cyclohexane, alcohol and isopropanol; however, when Fe₃O₄ was added into the

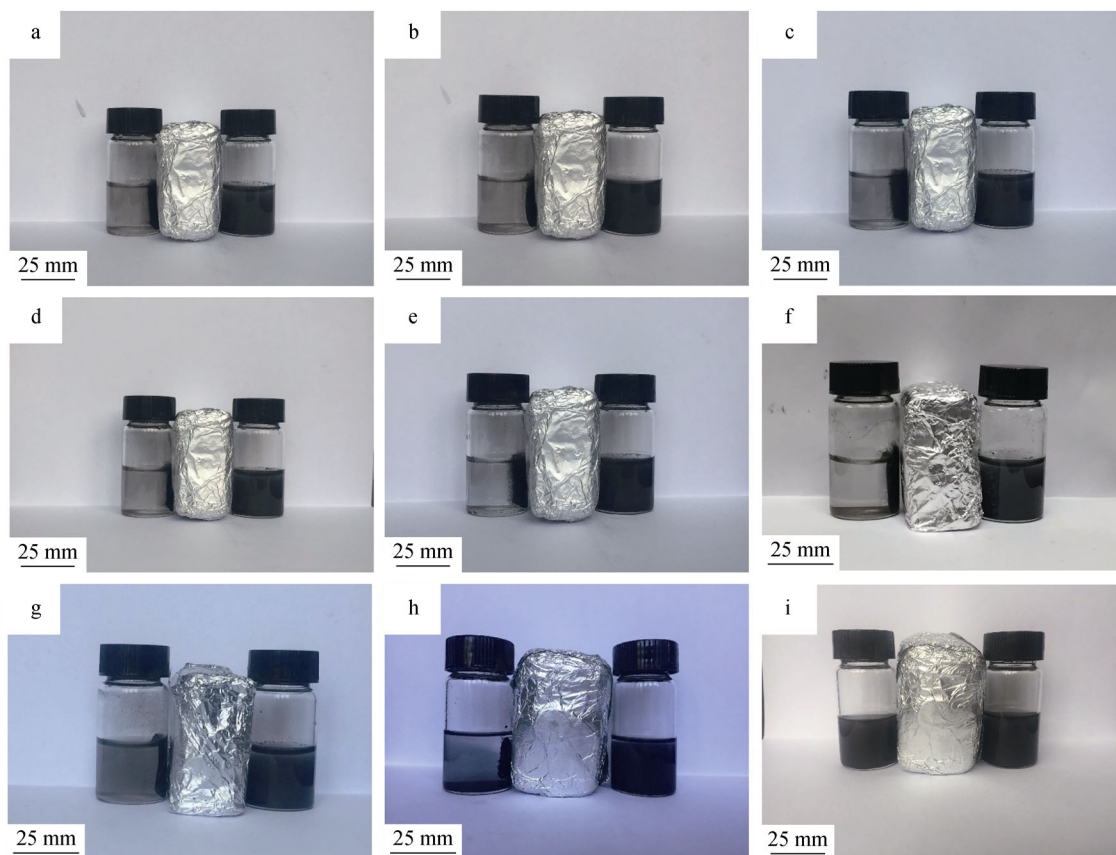


Fig. 6 Different mass ratios of $\text{Fe}_3\text{O}_4/\text{WS}_2$ in deionized water: **a** 0.25, **b** 0.50, **c** 1.00, **d** 1.50 and **e** 2.00; magnetic separation in different solvents: **f** deionized water, **g** cyclohexane, **h** alcohol and **i** isopropanol

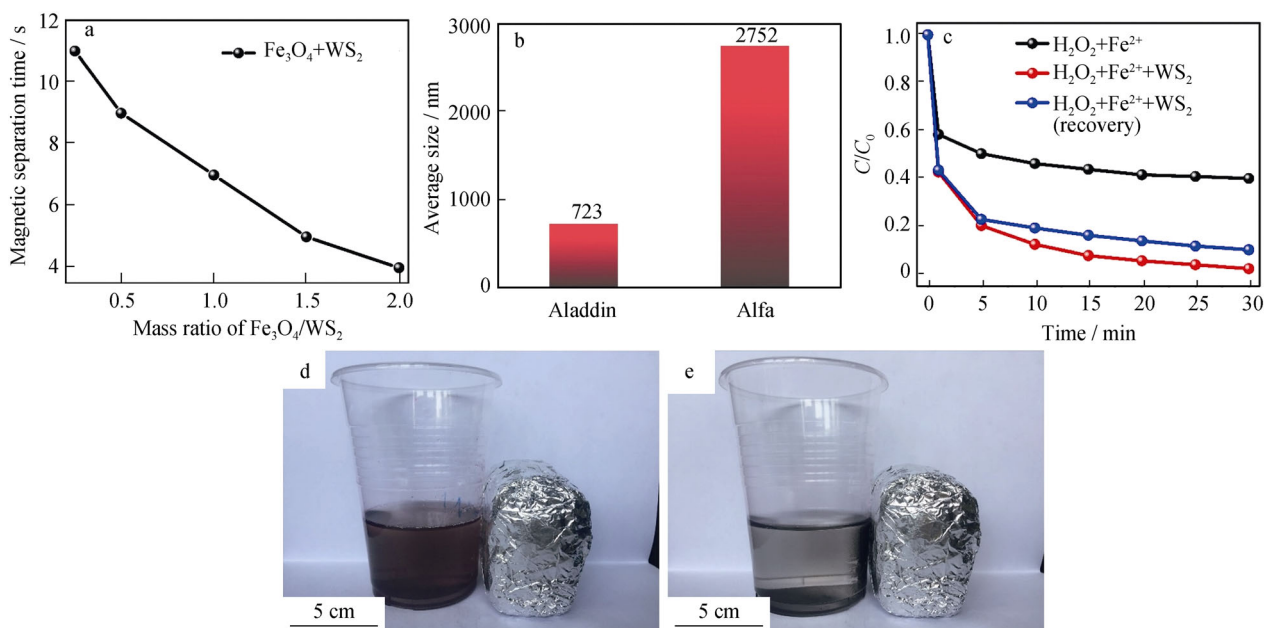


Fig. 7 **a** Variation of magnetic separation time with different mass ratios of $\text{Fe}_3\text{O}_4/\text{WS}_2$; **b** average size of MoS_2 from different manufacturers; **c** degradation of RhB in Fenton reaction with conditions of $0.4 \text{ mmol}\cdot\text{L}^{-1} \text{ H}_2\text{O}_2$, $20 \text{ mg}\cdot\text{L}^{-1} \text{ FeSO}_4\cdot 7\text{H}_2\text{O}$, $300 \text{ mg}\cdot\text{L}^{-1} \text{ WS}_2$, pH 4.0 (C/C_0 : concentration of l-RhB/initial concentration l-RhB); magnetic separation of WS_2 **d** before and **e** after adding Fe_3O_4

solution, WS₂ was successfully magnetically separated in deionized water, cyclohexane and alcohol, but failed to be recycled in isopropanol. Furthermore, it was noticed that the complete magnetic separation time of WS₂ and Fe₃O₄ was different in deionized water (3 s), cyclohexane (2 s) and alcohol (65 s). Thirdly, the particle size may be another factor affecting magnetic separation. Figure 7b shows the average sizes of MoS₂ bought from Aladdin and Alfa, which was 723 and 2752 nm, respectively. One of the possible reasons may be that the larger the particle size of MoS₂, the smaller the number of particles per unit mass, and the less the traction force provided by Fe₃O₄ was needed. Thus, MoS₂ (Alfa) could be magnetically separated better than MoS₂ (Aladdin) with the same mass of Fe₃O₄.

3.5 Application of magnetic separation in Fenton reaction

The rapid and efficient magnetic separation of metal sulfides/oxides was applied to Fenton reaction with metal sulfides/oxides as co-catalysts [46]. As shown in Fig. 7c, the degradation of RhB was greatly enhanced with WS₂ as a co-catalyst compared with traditional Fenton reaction, from 60.0% to 97.7% in 30 min. After reaction, the solution was turbid for the dispersion of WS₂ (Fig. 7d). Then, 5 mg Fe₃O₄ was added into the solution, and a few seconds later, the solution gradually became clear due to the magnetic separation of WS₂ with Fe₃O₄ (Fig. 7e). After the recovery of WS₂, Fenton reaction was performed again without any treatment on WS₂, and only a slight decrease on RhB degradation rate was observed, with 89.9% RhB degraded in 30 min, which was still higher and faster than traditional Fenton reaction. This result demonstrated that magnetic separation was a feasible method to separate metal sulfides/oxides.

4 Conclusion

The low separation efficiency of metal sulfides/oxides was solved by adding Fe₃O₄, and the mixture could be magnetic separated with an applied magnetic field. The mechanism was explored. The electrostatic force and the formation of chemical bonds were proved as the two main reasons to explain the magnetic separation phenomenon through mechanically mixing metal sulfides/oxides and Fe₃O₄. Different additions of Fe₃O₄ and different sizes of metal sulfides/oxides would influence the magnetic separation time and rate, and the magnetic separation could be applied in some organic solvent systems. Furthermore, as a characteristic metal sulfide, WS₂ was used as a co-catalyst in Fenton reaction, which could be magnetically separated

with Fe₃O₄ after reaction. We believe this study will provide a new perspective for rapid and highly efficient recovery of heterogeneous catalysts in many fields.

Acknowledgements This work was financially supported by the State Key Research Development Program of China (No. 2016YFA0204200), the National Natural Science Foundation of China (Nos. 21822603, 21773062, 21577036, 21377038 and 21237003), Shanghai Pujiang Program (No. 17PJ011) and the Fundamental Research Funds for the Central Universities (No. 22A201514021).

References

- [1] Zea H, Lester K, Datye AK, Rightor E, Gulotty R, Waterman W, Smith M. The influence of Pd–Ag catalyst restructuring on the activation energy for ethylene hydrogenation in ethylene–acetylene mixtures. *Appl Catal A-Gen.* 2005;282(1):237.
- [2] Cheng Z, Wang W, Yang LM, Xu Z, Ji ZG, Huang ST. Preparation of La-TiO₂ and photocatalytic degradation of petrochemical secondary effluent. *Chin. J. Rare Metals.* 2018; 42(9):950.
- [3] Jiang Z, Zhu K, Lin Z, Jin S, Guang L. Structure and Raman scattering of Mg-doped ZnO nanoparticles prepared by sol–gel method. *Rare Met.* 2018;37(10):881.
- [4] Zhao D, Liao Y, Zhang Z. Toxicity of ionic liquids. *Clean.* 2007; 35(1):42.
- [5] Carl Christoph T, Christian M, Willi B, Sebastian R, André H, Rainer H. Modern separation techniques for the efficient workup in organic synthesis. *Angew Chem Int Ed.* 2010;41(21):3964.
- [6] Barbaro P, Liguori F, Linares N, Marrodan CM. Heterogeneous bifunctional metal/acid catalysts for selective chemical processes. *Eur J Inorg Chem.* 2012;2012(24):3807.
- [7] Anipsitakis GP, Dionysiou DD. Radical generation by the interaction of transition metals with common oxidants. *Environ Sci Technol.* 2004;38(13):3705.
- [8] Nadkarni SV, Gawande MB, Jayaram RV, Nagarkar JM. Synthesis of bis(indolyl)methanes catalyzed by surface modified zirconia. *Catal Commun.* 2008;9(8):1728.
- [9] Fang W, Zhou L, Shen B, Zhou Y, Yi Q, Xing M, Zhang J. Advanced visible-light-driven activity for the degradation of organic dyes. *Res Chem Intermed.* 2018;44(8):4609.
- [10] Liu Q, Shen J, Hua T, Zhang T, Yang X. 3D Reduced graphene oxide aerogel-mediated Z-scheme photocatalytic system for highly efficient solar-driven water oxidation and removal of antibiotics. *Appl Catal B-Environ.* 2018;232:562.
- [11] Yang X, Tian L, Zhao X, Tang H, Liu Q, Li G. Interfacial optimization of g-C₃N₄-based Z-scheme heterojunction toward synergistic enhancement of solar-driven photocatalytic oxygen evolution. *Appl Catal B-Environ.* 2019;244:240.
- [12] Svoboda J. *Magnetic Techniques for the Treatment of Materials.* Berlin: Springer; 2004. 1.
- [13] Svoboda J, Fujita T. Recent developments in magnetic methods of material separation. *Miner Eng.* 2003;16(9):785.
- [14] Hillier S, Hodson ME. High-gradient magnetic separation applied to sand-size particles; an example of feldspar separation from mafic minerals. *J Sediment Res.* 1997;67(5):975.
- [15] Kolm H, Oberteuffer J, Kelland D. High-gradient magnetic separation. *Sci Am.* 1975;233(5):46.
- [16] Fletcher D. Fine particle high gradient magnetic entrapment. *IEEE Trans Magn.* 1991;27(4):3655.

- [17] Hubbuch JJ, Matthiesen DB, Hobley TJ, Thomas OR. High gradient magnetic separation versus expanded bed adsorption: a first principle comparison. *Bioseparation*. 2001;10(1):99.
- [18] Moeser GD, Roach KA, Green WH, Alan Hatton T, Laibinis PE. High-gradient magnetic separation of coated magnetic nanoparticles. *AIChE J*. 2004;50(11):2835.
- [19] Majewski P, Thierry B. Functionalized magnetite nanoparticles—synthesis, properties, and bio-applications. *Crit Rev Solid State*. 2007;32(3–4):203.
- [20] Ngomsik AF, Bee A, Draye M, Cote G, Cabuil V. Magnetic nano- and microparticles for metal removal and environmental applications: a review. *Comptes Rendus Chim*. 2005;8(6):963.
- [21] Menini L, Pereira MC, Parreira LA, Fabris JD, Gusevskaya EV. Cobalt- and manganese-substituted ferrites as efficient single-site heterogeneous catalysts for aerobic oxidation of monoterpenic alkenes under solvent-free conditions. *J Catal*. 2008;254(2):355.
- [22] Stein M, Wieland J, Steurer P, Tölle F, Mülhaupt R, Breit B. Iron nanoparticles supported on chemically-derived graphene: catalytic hydrogenation with magnetic catalyst separation. *Adv Synth Catal*. 2011;353(4):523.
- [23] Rossi LM, Costa NJS, Silva FP, Wojcieszak R. Magnetic nanomaterials in catalysis: advanced catalysts for magnetic separation and beyond. *Green Chem*. 2014;16(6):2906.
- [24] Safarik I, Safarikova M. Magnetic techniques for the isolation and purification of proteins and peptides. *Biomagn Res Technol*. 2004;2(1):7.
- [25] Hajian R, Ehsanikah A. Manganese porphyrin immobilized on magnetic MCM-41 nanoparticles as an efficient and reusable catalyst for alkene oxidations with sodium periodate. *Chem Phys Lett*. 2018;691:146.
- [26] Ma Q, Cui Y, Deng X, Li B, Cheng Q, Cheng X. Fabrication of magnetic TiO₂ nano-catalyst and its enhanced photocatalytic and recycle performance. *J Nanosci Nanotechnol*. 2017;17(3):2019.
- [27] Chang YC, Chen DH. Preparation and adsorption properties of monodisperse chitosan-bound Fe₃O₄ magnetic nanoparticles for removal of Cu(II) ions. *J Colloid Interface Sci*. 2005;283(2):446.
- [28] Liu JF, Zhao ZS, Jiang GB. Coating Fe₃O₄ magnetic nanoparticles with humic acid for high efficient removal of heavy metals in water. *Environ Sci Technol*. 2008;42(18):6949.
- [29] Hudlet S, Jean MS, Roulet B, Berger J, Guthmann C. Electrostatic forces between metallic tip and semiconductor surfaces. *J Appl Phys*. 1995;77(7):3308.
- [30] Martín A, Martínez F, Malfeito J, Palacio L, Prádanos P, Hernández A. Zeta potential of membranes as a function of pH: optimization of isoelectric point evaluation. *J Membr Sci*. 2003;213(1):225.
- [31] Igor C, Laurence DE, Lazare NO, Jean-François F, Simone CJ, Martin S, Hervé M, Pierre D. Molecular composition of iron oxide nanoparticles, precursors for magnetic drug targeting, as characterized by confocal Raman microspectroscopy. *Analyst*. 2005;130(10):1395.
- [32] Zeng W, Feng LP, Su J, Pan HX, Liu ZT. Layer-controlled and atomically thin WS₂ films prepared by sulfurization of atomic-layer-deposited WO₃ films. *J Alloy Compd*. 2018;745:834.
- [33] Rezaee M, Khoie SMM, Liu KH. The role of brookite in mechanical activation of anatase-to-rutile transformation of nanocrystalline TiO₂: an XRD and Raman spectroscopy investigation. *CrystEngComm*. 2011;13(16):5055.
- [34] Xu S, Sun J, Weng L, Hua Y, Liu W, Neville A, Hu M, Gao X. In-situ friction and wear responses of WS₂ films to space environment: vacuum and atomic oxygen. *Appl Surf Sci*. 2018;447:368.
- [35] Yen PC, Huang YS, Tiong KK. The growth and characterization of rhenium-doped WS₂ single crystals. *J Phys: Condens Matter*. 2004;16(12):2171.
- [36] Yang L, Majumdar K, Liu H, Du Y, Wu H, Hatzistergos M, Hung PY, Tieckelmann R, Tsai W, Hobbs C. Chloride molecular doping technique on 2D materials: WS₂ and MoS₂. *Nano Lett*. 2014;14(11):6175.
- [37] Karikalan N, Karthik R, Chen SM, Karuppiyah C, Elangovan A. Sonochemical synthesis of sulfur doped reduced graphene oxide supported CuS nanoparticles for the non-enzymatic glucose sensor applications. *Sci Rep*. 2017;7(1):2494.
- [38] Wang Q, Ning A, Yan B, Hang H, Li J, Lu X, Liu Y, Wang F, Li Z, Lei Z. High photocatalytic hydrogen production from methanol aqueous solution using the photocatalysts CuS/TiO₂. *Int J Hydrog Energy*. 2013;38(25):10739.
- [39] Wen Z, Shao P, Ci S, Yi L, Cai P, Huang P, Cao C. Hollow CuS microcube electrocatalysts for CO₂ reduction reaction. *Chem-electrochem*. 2017;4(10):2593.
- [40] Zhang S, Hongyu LI, Qin Z. Promotional effect of F-doped V₂O₅-WO₃/TiO₂ catalyst for NH₃-SCR of NO at low-temperature. *Appl Catal A-Gen*. 2012;435(17):156.
- [41] Wang J, Chen Y, Zhou W, Tian G, Xiao Y, Fu H, Fu H. Cubic quantum dot/hexagonal microsphere ZnIn₂S₄ heterophase junction for exceptional visible-light-driven photocatalytic H₂ evolution. *J Mater Chem A*. 2017;5(18):8451.
- [42] Zhang Q, Hu S, Fan Z, Liu D, Zhao Y, Ma H, Li F. Preparation of g-C₃N₄/ZnMoCdS hybrid heterojunction catalyst with outstanding nitrogen photofixation performance under visible light via hydrothermal post-treatment. *Dalton Trans*. 2016;45(8):3497.
- [43] Qi D, Lu L, Xi Z, Wang L, Zhang J. Enhanced photocatalytic performance of TiO₂ based on synergistic effect of Ti³⁺ self-doping and slow light effect. *Appl Catal B-Environ*. 2014;160(6):621.
- [44] Li K, Gao S, Wang Q, Xu H, Wang Z, Huang B, Dai Y, Lu J. In-situ-reduced synthesis of Ti³⁺ self-doped TiO₂/g-C₃N₄ heterojunctions with high photocatalytic performance under LED light irradiation. *ACS Appl Mater Interfaces*. 2015;7(17):9023.
- [45] An L, Li Y, Luo M, Yin J, Zhao YQ, Xu C, Cheng F, Yang Y, Xi P, Guo S. Atomic-level coupled interfaces and lattice distortion on CuS/NiS₂ nanocrystals boost oxygen catalysis for flexible Zn-air batteries. *Adv Funct Mater*. 2017;27(42):1703779.
- [46] Xing M, Xu W, Dong C, Bai Y, Zeng J, Zhou Y, Zhang J, Yin Y. Metal sulfides as excellent co-catalysts for H₂O₂ decomposition in advanced oxidation processes. *Chem*. 2018;4(6):1359.